



## Tsunami Simulation Using Computed Ground Motion of the 2011 Tohoku Earthquake

S. Akiyama<sup>(1)</sup>, M. Korenaga<sup>(2)</sup>, K. Kawaji<sup>(3)</sup>

<sup>(1)</sup> ITOCHU Techno-Solutions Corporation, [shinichi.akiyama@ctc-g.co.jp](mailto:shinichi.akiyama@ctc-g.co.jp)

<sup>(2)</sup> ITOCHU Techno-Solutions Corporation, [mariko.korenaga@ctc-g.co.jp](mailto:mariko.korenaga@ctc-g.co.jp)

<sup>(3)</sup> ITOCHU Techno-Solutions Corporation, [kaoru.kawaji@ctc-g.co.jp](mailto:kaoru.kawaji@ctc-g.co.jp)

### Abstract

A tsunami simulation is carried out using seabed displacement as initial tsunami-water level, which is obtained from a ground-motion simulation for the 2011 Tohoku Earthquake. First, a large scale ground-motion simulation is performed for the whole Eastern Japan with a voxel type finite-element method. Two types of seismic source model are adopted in the ground-motion simulation. One is derived from an inversion analysis based on teleseismic data, the other is derived on strong-motion data. Simulated ground-motion waveforms generally correspond to the observed ones at K-NET and KiK-net stations in the Eastern Japan. Second, a tsunami simulation is executed by a finite-difference method based on the shallow-water theory. Simulated tsunami waveforms are roughly consistent with observed ones of GPS wave gauges deployed off the Pacific coast of Tohoku. Coastal tsunami heights in the Sendai Plain and inundation around the Soma Port simulated by the source models based on the teleseismic and the strong-motion data are well consistent with observed ones, because large slips are generated on deep part of the fault plane in both models appropriately. However, the tsunami heights in the Sanriku coast simulated by the source model based on the teleseismic data are fairly lower than the observed heights, because the slip near the Japan Trench in this model is not so large. On the other hand, the simulated heights based on the strong-motion data correspond with the observed ones, because there is a huge slip near the trench axis in this model. A large slip on shallow part of the fault plane near the trench axis, which affects large tsunami heights in the Sanriku coast, is hard to be detected by the seismic observation, because of lack of strong ground-shaking in its observation. It is desirable to reproduce the large slip near the trench axis by the weak ground-shaking caught in the teleseismic or the strong-motion observation with higher accuracy.

*Keywords: tsunami; ground motion; the 2011 Tohoku Earthquake; source model; numerical simulation*

### 1. Introduction

Fault slip under seabed causes ground motion and leads to tsunami due to deformation of the ocean floor. Therefore, it is natural to evaluate both ground motion and tsunami by using a single source model. However, the ground motion and the tsunami are assessed separately by different source models in practice, because it is really difficult to evaluate both phenomena by one source model.

Study on source-process inversion using seismic or tsunami observation data is recently improved in accordance with enhancement of their observation systems which include K-NET [1], KiK-net [2], the tsunami observation systems with GPS wave gauges and the sea water-pressure gauges. Many source models for the 2011 off the Pacific coast of Tohoku Earthquake (Mw9.0, we call it “the 2011 Tohoku Earthquake” in this paper) are proposed from the source inversion based on a large number of records for seismic and tsunami observations (e.g. [3, 4, 5, 6, 7]). Most of these models have a common feature that a large slip occurs on east side of the hypocenter near the Japan Trench. It suggests a possibility to evaluate the ground motion and the tsunami simultaneously using a single source model. We focus on tsunami prediction using a source model obtained from seismic observation.

In previous tsunami simulation, an initial water level for the tsunami has been treated to be equal to a static displacement of seabed often derived from a solution of elastic theory (e.g. [8]), while a dynamic displacement has not been taken into account in the tsunami simulation. Now, we take note of the influence of the dynamic

displacement on the tsunami evaluation, because the tsunami is generated by dynamic fault slip. Ohmachi et al. (2001) [9] developed a simulation method for tsunami excited by the dynamic displacement of seabed due to dynamic fault slip. In their method, the tsunami is evaluated to solve three-dimensional (3-D) Navier-Stokes equation with a finite-difference method applying the dynamic displacement which is calculated by a boundary-element method. Using their method, they evaluated the tsunami heights that attacked Okushiri Island in the 1993 South-West off Hokkaido Earthquake. Furumura and Saito (2009) [10] also developed a method simulating ground-motion and tsunami simultaneously by solving both 3-D equation of motion for an elastic body and 3-D Navier-Stokes equation with a finite-difference method. They simulate the ground motion and the tsunami for the 1944 Tonankai Earthquake using a parallel computing with a super-computer. Their studies show that both the ground motion and the tsunami can be computed at the same time from one source model. However, they do not argue about the validity of the tsunami prediction by using the seismic source model.

In this study, the seabed displacement due to the 2011 Tohoku Earthquake is calculated by the ground-motion simulation. The source model is provided by the source-process inversion using the seismic observation data. Then, we perform the tsunami simulation using the computed seabed displacement as an initial water level. The tsunami simulation is carried out by a finite-difference method based on the shallow-water theory. Finally, we investigate about the tsunami evaluation using the source model based on the seismic observation data. We have already calculated the tsunami waveforms at GPS wave gauge stations deployed off the Pacific coast of Tohoku using the seismic source models derived from the inversion analyses for the teleseismic data and the strong ground-motion data, respectively [11, 12]. In this paper, we also present the computed tsunami heights and inundation along the coast of Tohoku in detail, and discuss the potentiality on the tsunami prediction using the seismic source model based on the teleseismic or the strong-motion data, including our previous studies.

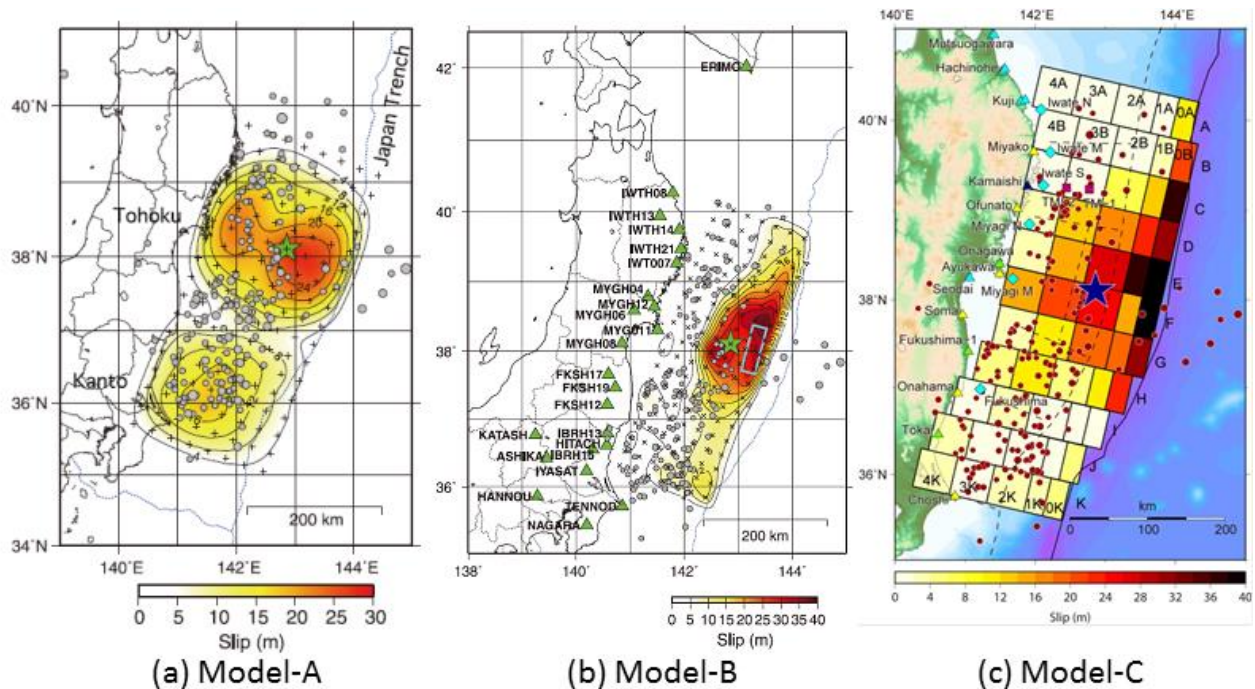


Fig.1 Source models for the 2011 Tohoku Earthquake. (a) Model-A is the inversion of the teleseismic data and (b) Model-B is the inversion of the regional strong-motion data. Both are derived from Yoshida et al. (2011) [5]. (c) Model-C is the inversion of the tsunami data by Satake et al. (2013) [6].

## 2. Comparison of the source models

Many source models are presented based on the inversion analysis using seismic or tsunami observation data after the 2011 Tohoku Earthquake. As an example, Fig.1 shows three source models formed by the seismic and tsunami observation data. Model-A is obtained from the inversion using the teleseismic data and Model-B is



from the regional strong-motion data. Both are proposed by Yoshida et al. (2011) [5]. On the other hand, Model-C is derived from the tsunami observation data by Satake et al. (2013) [6]. The three models have a common feature that the largest slip about 30-40 m is seen on east side of the hypocenter and close to the Japan Trench. It suggests a possibility to evaluate the ground motion and the tsunami simultaneously from one source model. However, the slip distribution is different among the three models. So we compare Model-A and Model-B with Model-C in detail, because Model-C reportedly reproduces the tsunami observation with accuracy.

The slip distribution of Model-C mainly spreads out from the hypocenter. The largest slip is over 40m on east of the hypocenter along the Japan Trench. The other slips are distributed with 10-20 m near the coast of Miyagi and with 5-10 m on south than the offshore of Fukushima. Next, the largest slip of Model-A is about 30 m that is smaller than one of Model-C. The slip on west of the hypocenter is about 20 m which is similar to one of Model-C. On the other hand, the slip distribution near the Japan Trench is not slender like one of Model-C. The slip distribution on the south part also is not similar to one of Model-C. At last, a large slip of Model-B distributed along the Japan Trench is similar to one of Model-C. The largest slip is about 40 m that is similar to one of Model-C. However, the slip distribution on west side of the hypocenter spreads smaller than one of Model-C. In above comparison between Model-A and Model-B, we cannot find which model is better to reproduce the tsunami. Therefore, we adopt both Model-A and Model-B in this study to investigate what these common or different features affect the tsunami evaluation.

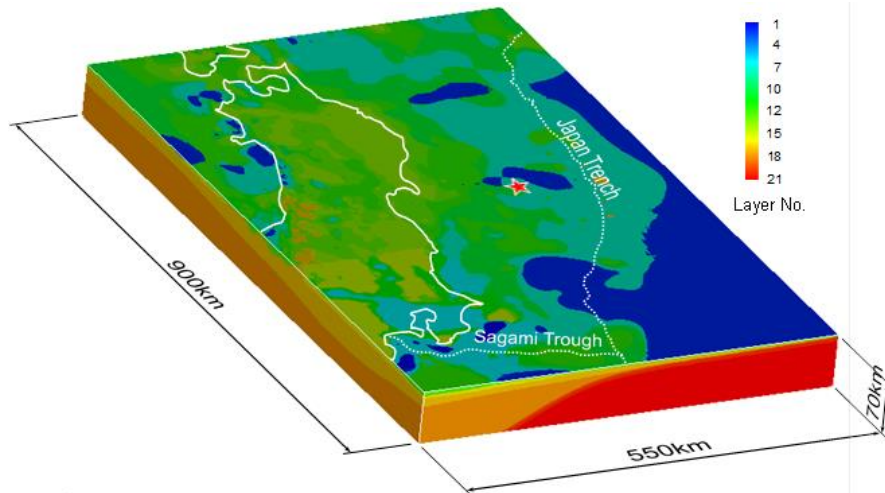


Table 1 Properties of the layer shown in Fig.2

Layer No.	$V_p$ (km/s)	$V_s$ (km/s)	$\rho$ ( $g/cm^3$ )	$Q_p$	$Q_s$
1	1.70	0.35	1.80	119	70
2	1.80	0.50	1.95	170	100
3	2.00	0.60	2.00	204	120
4	2.10	0.70	2.05	238	140
5	2.20	0.80	2.07	272	160
6	2.30	0.90	2.10	306	180
7	2.40	1.00	2.15	340	200
8	2.60	1.10	2.20	374	220
9	2.70	1.30	2.20	442	260
10	3.00	1.50	2.25	510	300
11	3.20	1.70	2.30	578	340
12	3.50	2.00	2.35	680	400
13	4.20	2.40	2.45	680	400
14	5.00	2.90	2.60	680	400
15	5.50	3.20	2.65	680	400
16	5.80	3.42	2.70	680	400
17	6.40	3.82	2.90	680	400
18	7.50	4.48	3.20	850	500
19	5.40	2.78	2.60	340	200
20	6.50	3.48	2.80	510	300
21	8.10	4.60	3.40	850	500

Fig.2 3-D subsurface structure model covering the Eastern Japan and including the hypocenter for the 2011 Tohoku Earthquake. Gradation of color shows the layer number. Red symbol shows the hypocenter.

### 3. Ground-motion simulation for the 2011 Tohoku Earthquake

A ground-motion simulation for a large area covering the Eastern Japan due to the 2011 Tohoku Earthquake is aimed to obtain the seabed displacement which is applied to a tsunami simulation described later. In this simulation, we use a voxel type finite-element method [13] to take account of the 3-D subsurface structure.

The Eastern Japan including the hypocenter in the Pacific Ocean is modelled based on the Japan Integrated Velocity Model [14]. Fig.2 shows the simulation model covering the Eastern Japan extending to 550 km (east-west)  $\times$  900 km (north-south)  $\times$  70 km (depth). Gradation of color shows the layer number indicated in Table 1. This simulation model is constructed by approximately 1 billion voxel elements that size is 250 m and 500 m.

Both Model-A and Model-B shown in Fig.1 are adopted as the seismic source in this simulation. We divide the fault plane of Model-A (480 km  $\times$  270 km) into subfaults with 30 km  $\times$  30 km, and use a smoothed ramp function as the source time function on every subfault. The fault slip is assumed to propagate circularly from the hypocenter. On the other hand, the fault plane of Model-B (475 km  $\times$  175 km) is divided into subfaults with 25 km  $\times$  25 km. We set the moment rate function and the slip propagation which are derived from the seismic inversion by Yoshida et al. (2011) [5].

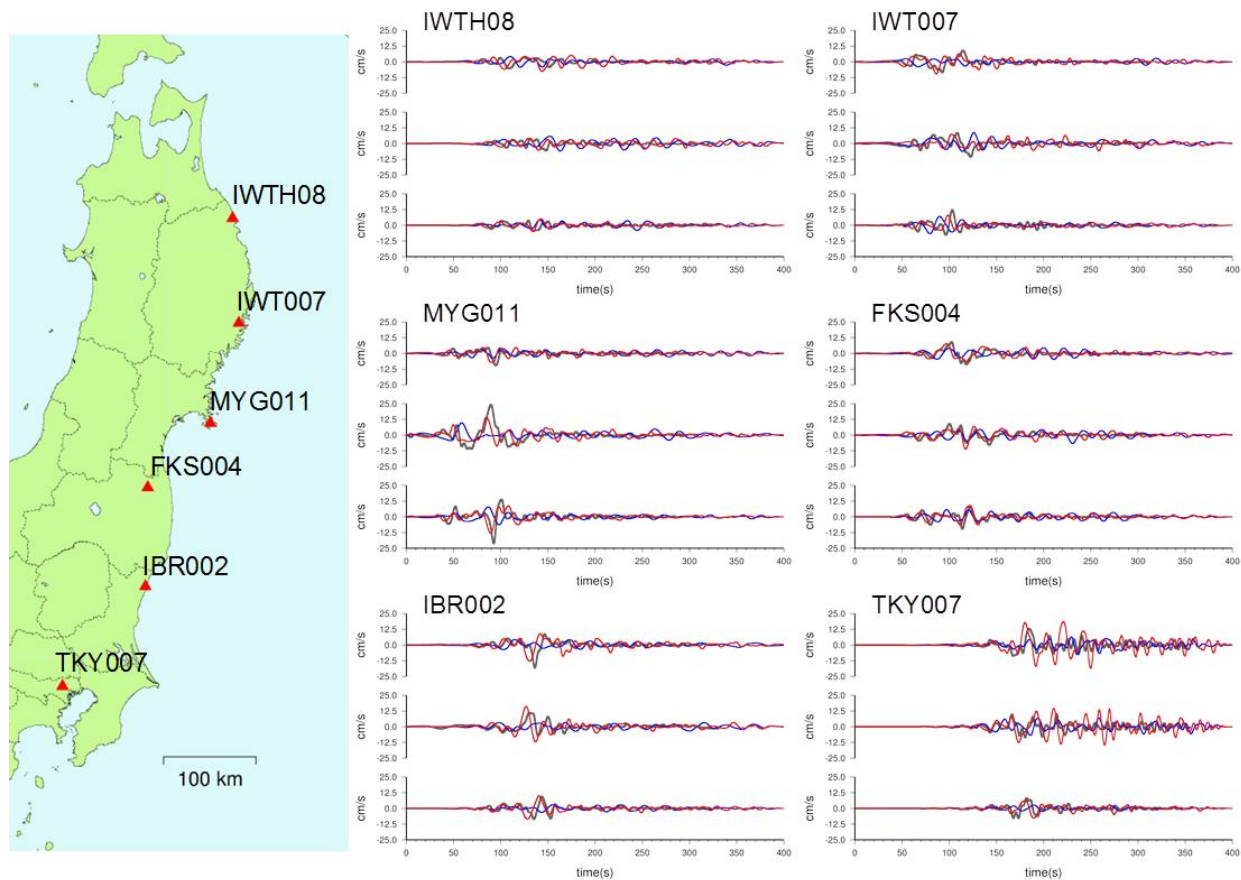


Fig.3 Comparison of simulated and observed velocity waveforms at K-NET and KiK-net stations. Blue and red lines indicate the waveforms from Model-A and Model-B, respectively. Gray lines indicate observed waveforms. N-S, E-W and U-D components are shown in upper, middle and lower graphs, respectively. The waveforms are processed by the band pass filter that period range is 7-50 s.

Fig.3 shows comparison between simulated and observed velocity waveforms. The simulated waveforms from Model-A and Model-B almost accord with the observed ones for arrival time, amplitude and phase of the seismic wave in every station. In detail, some of the peaks seen in the observed waveforms are not reproduced by the simulation with Model-A, while those are well reproduced by the simulation with Model-B. These results suggest that Model-B based on the strong-motion data contains more detailed information about the source fault than Model-A based on the teleseismic data. It is confirmed in Fig.3 that two types of the ground-motion simulations are performed appropriately.

#### 4. Computed vertical displacement

Vertical displacements computed by two types of the ground-motion simulations are picked up to summarize their characteristics. The simulation code with the voxel type finite-element method has already been verified by Koketsu et al. (2004) [13] that the calculated displacement in an elastic half space is equal to the theoretical solution by Okada (1985) [8]. We start the following discussion, accepting the computation scheme is confirmed.

The ground motion is simulated during 400 s after the earthquake strikes. We assume the computed dynamic displacement at 400 s as a permanent displacement. Fig.4 shows vertical component of the permanent displacement obtained by the ground-motion simulation based on Model-A and Model-B, respectively. It is found as a common feature that the largest uplift appears on east side of the hypocenter in both Fig.4 (a) and (b). However, several different features are also seen between (a) and (b). Uplifts arise on west and south side of the hypocenter in (a). On the other hand, the uplift on east side of the hypocenter is long and narrow along the Japan Trench and the subsidence is seen on west side of the hypocenter in (b). These differences appear to depend on

the slip distribution on the source models shown in Fig.1. Although, there are several differences between Fig.4 (a) and (b), their vertical displacement distributions are calculated appropriately, because they are roughly consistent with the slip distribution shown in Fig.4 (c) by Ozawa et al. (2011) [7].

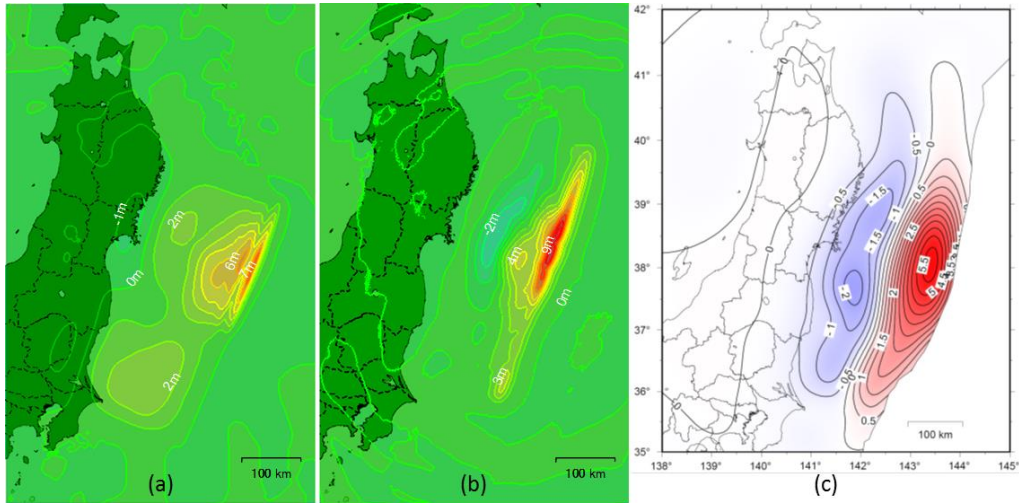


Fig.4 Distribution of the vertical component of the permanent displacement in the seabed by the ground-motion simulation (a) Result from Model-A (b) Result from Model-B. (c) Calculated vertical displacements by Ozawa et al. (2011) [7]

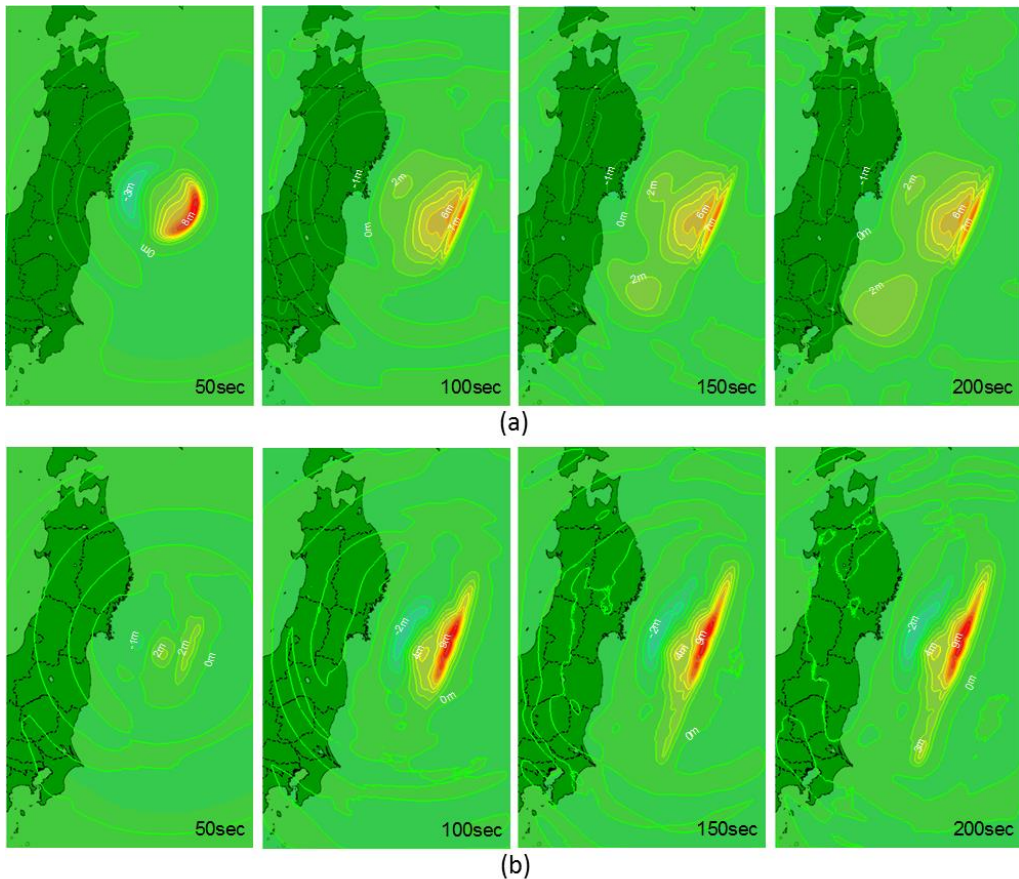


Fig.5 Snapshot of vertical displacement distribution in the seabed by the ground-motion simulation. (a) Results from Model-A. (b) Results from Model-B.

Fig.5 shows snapshots of the vertical displacement distribution. In Fig.5 (a), uplift near the hypocenter grows rapidly during 50 s after the earthquake strikes, and converges constantly to 100 s. In addition, another uplift is generated on south of the hypocenter after 100 s. In Fig.5 (b), a large uplift occurs near the hypocenter between 50 s and 100 s and spreads slender to the south direction after 100 s. Deformations of the seabed in Fig.5 (a) and (b) converge at the 200 s when the fault slip stops. The vertical displacements of the seabed shown in Fig.5 are used in the tsunami simulation described in the next section.

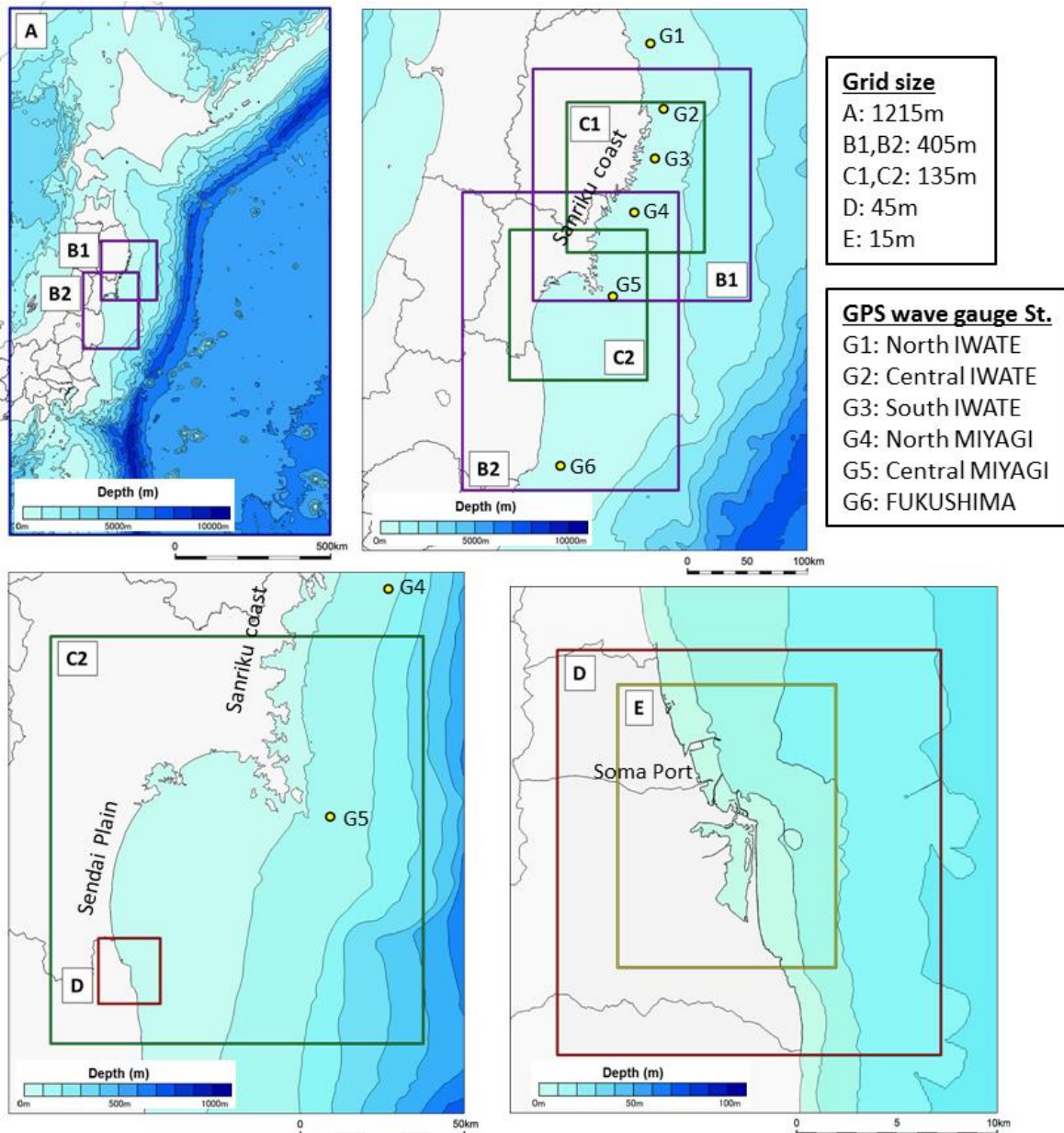


Fig.6 Seabed topography and tsunami-simulation model with various grid sizes.

## 5. Tsunami simulation

We carry out the tsunami simulation using the vertical displacement described in the former section as the initial water level of tsunami. A finite-difference method based on the shallow-water theory [15] is adopted in the tsunami simulation. The seabed topography of the Pacific Ocean targeted by the simulation is modeled based on the grid data of M7000 series provided by Japan Coast Guard and J-TOPO30 by Marine Information Research



Center. The model of the seabed topography is shown in Fig.6. In the tsunami simulation, several grid sizes are used with a nesting technique to compute tsunami waveforms, coastal tsunami heights and inundation heights. Fig.6 also describes several regions according to the grid size for the tsunami simulation. The region A whose grid size is 1215 m is used for the tsunami simulation in the whole Eastern Japan including a hypocenter of the earthquake. The region C (C1 and C2) whose grid size is 135 m is used for the detailed computation of the tsunami heights along the Sanriku coast and the Sendai Plain. We also use the region E whose grid size is 15m for calculating the inundation heights around the Soma Port.

Two types of computed vertical displacements are used in this tsunami simulation; one is obtained by the ground-motion simulation with Model-A based on the teleseismic data shown in Fig.1, the other by Model-B based on the strong-motion data. Tsunami propagation is calculated to 18,000 steps at time interval of 1 s (duration time is 5 hours). We start the simulation at the static water level before the earthquake occurrence as the initial condition, and calculate the tsunami heights adding the increment of displacement in the seabed shown in Fig.6 as the fluctuation of the water level at every 5 s for 200 s when the fault slip converges. First, we investigate reproducibility of the tsunami waveform by the tsunami simulation with the seismic source model, comparing with the observation at the GPS wave gauge stations shown in Fig.6. Next, we discuss the coastal tsunami heights and the inundation on land calculated from the tsunami simulation, focusing on relation with the slip distribution of the seismic source model.

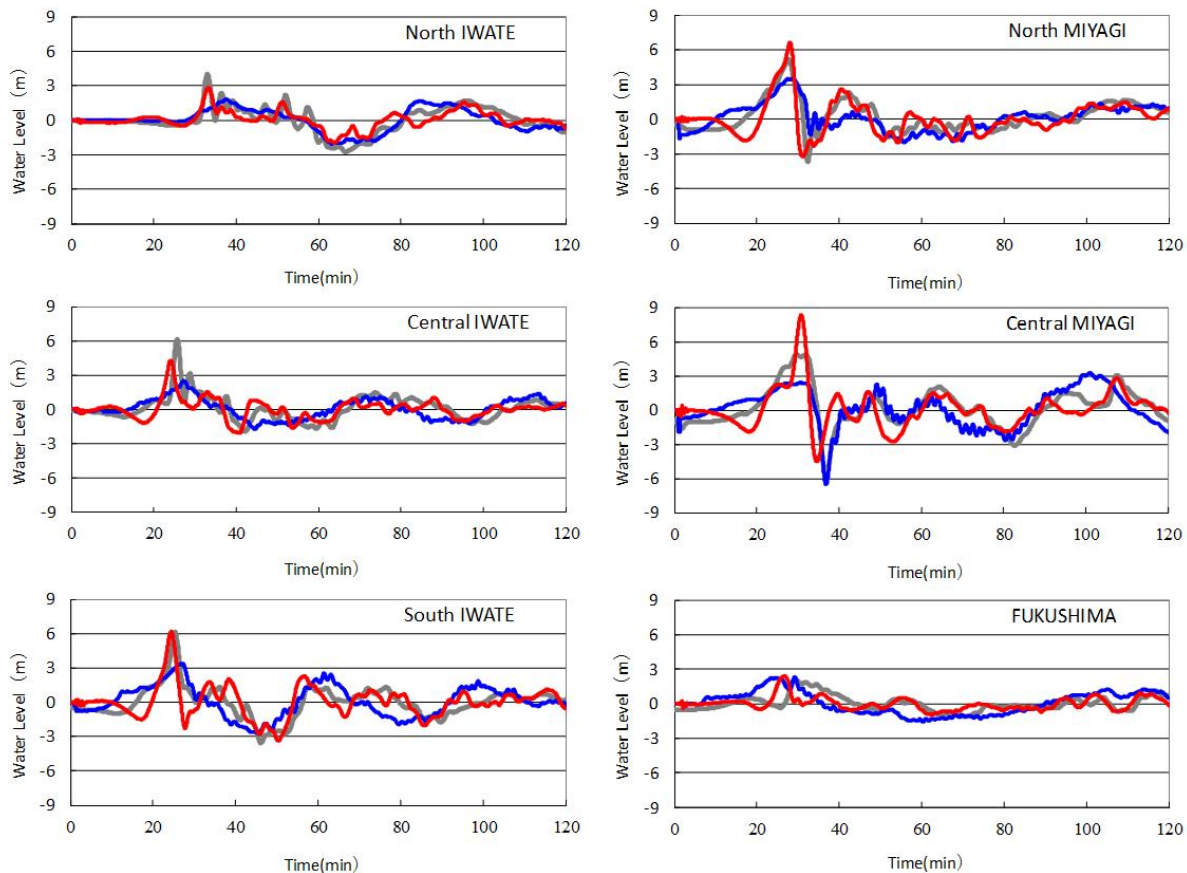


Fig.7 Comparison between simulated and observed waveforms at the GPS wave gauge stations. Blue and red lines represent the simulated waveforms based on Model-A and Model-B, respectively. Gray lines represent the observed tsunami waveforms.

## 6. Tsunami waveforms at GPS wave gauge stations

Fig.7 shows the calculated waveforms from the tsunami simulation and the observed waveforms at the GPS wave gauge stations. The tsunami simulation is carried out in the region A. The calculated waveforms from the



Model-A and Model-B are roughly consistent with the GPS wave gauge data on the 6 observation stations shown in Fig.6, for the amplitude and the arrival time of the peak of the waveforms. However, the calculated waveforms are slightly different from the observed ones, if we note the first arrival that shows the highest water level.

Focusing the observed waveforms at the 3 GPS stations off Iwate, the first arrival is formed by the short period wave (the period is approximately 10 min) and the long period wave (the period approximately 40 min). We can point out two features for the simulated tsunami waveforms; one, the calculated waveforms from Model-A based on the teleseismic data correspond with the long period component of the observed waveforms, the other, the calculated waveforms from Model-B based on the strong-motion data are consistent with the short period component of the observed waveforms. Satake et al. (2013) [6] indicate that the slip on deep part of the plate causes a long period tsunami wave and the slip on shallow part near the trench axis causes a short period wave in the 2011 Tohoku Earthquake. According to their indications, a long-period component excels in the computed tsunami wave from Model-A, because the effect of the slip on the deep part of the fault plane appears on it more strongly. On the other hand, the computed tsunami wave from Model-B emphasizes a short-period component, because it is affected more greatly by the slip on the shallow part of the fault plane near the Japan Trench. These features also appear at the GPS stations off Miyagi and Fukushima. The results described here suggest the ability to evaluate the tsunami prediction by using the seismic source model.

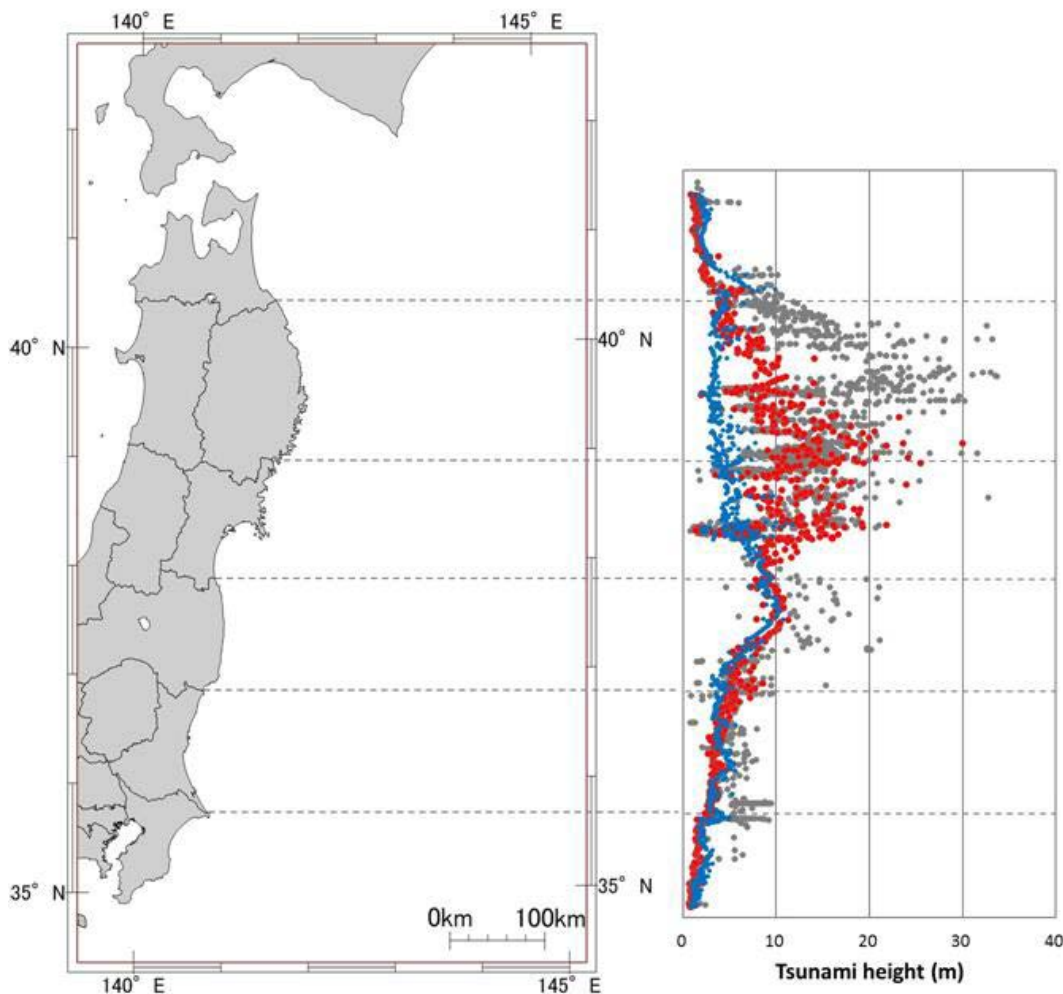


Fig.8 Comparison between simulated and observed tsunami heights along the Pacific coast of the Eastern Japan. Blue and red symbols represent the simulated tsunami heights from Model-A and Model-B, respectively. Gray symbol represents the observed tsunami heights.

## 7. Coastal tsunami height and inundation

Fig.8 shows the coastal tsunami heights computed from two types of the tsunami simulations, comparing with the observation data measured by Japan Tsunami Trace Database [16]. The computed tsunami heights shown in Fig.8 are obtained by the simulation in the region A (a grid size is 1215 m), to examine roughly the distribution of the coastal tsunami heights. The tsunami heights of the observed data indicate over 30 m in north of the Sanriku coast. The tsunami heights computed from Model-A based on the teleseismic data show less than 10 m in this area. On the other hand, the computed tsunami heights from Model-B based on the strong-motion data indicate 20-30 m, which are close to the observed heights in middle of the Sanriku coast, but are lower than the observed ones in north of the Sanriku coast. On the contrary, the computed tsunami heights from both Model-A and Model-B correspond with the observed ones in south than the Sendai Plain.

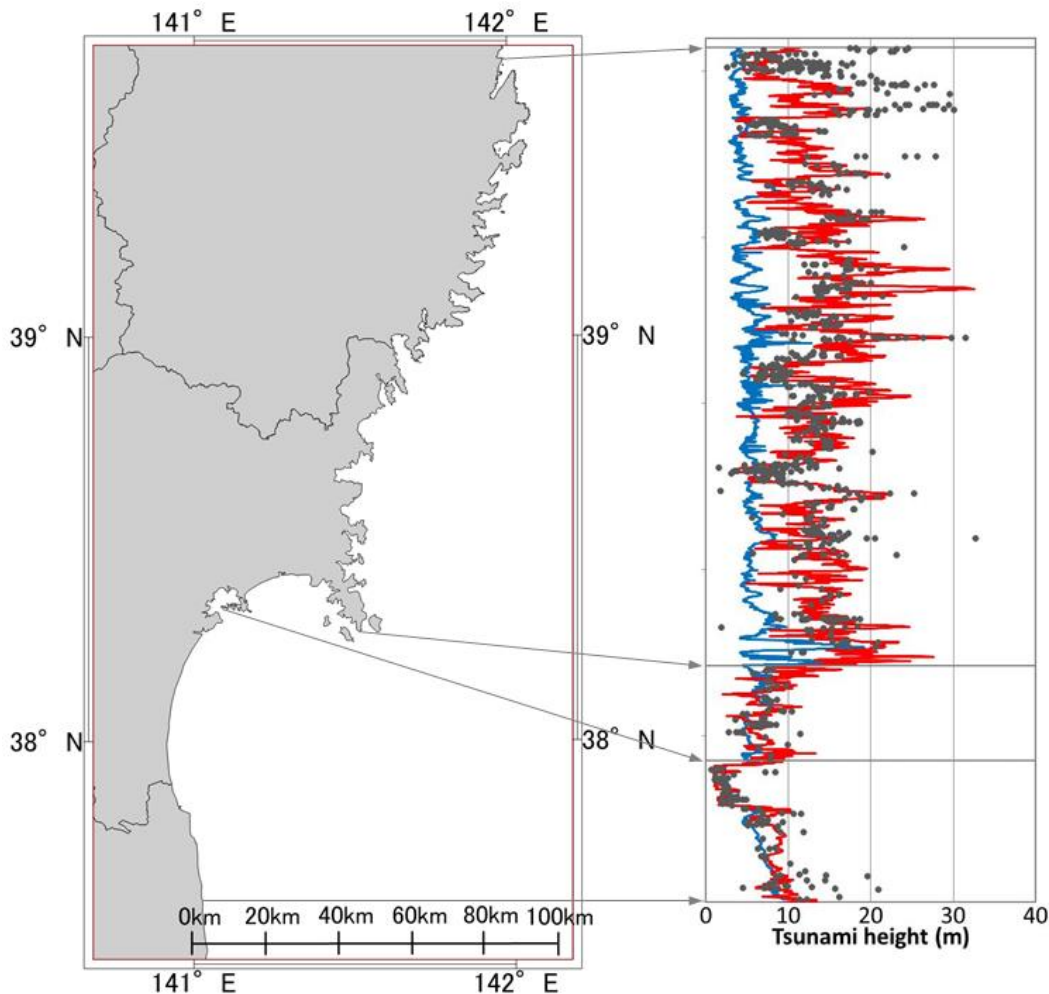


Fig.9 Comparison between simulated and observed maximum tsunami heights along the Pacific coast of Tohoku. Blue and red lines represent the simulated tsunami heights based on Model-A and Model-B, respectively. Gray symbol represents the observed tsunami heights.

In Fig.9, we present the coastal tsunami heights from the Sanriku coast to the Sendai Plain obtained from the tsunami simulation in the region C1 and C2 whose grid sizes are both 135 m, to compare with the observed heights in more detail. The coastal tsunami heights from the tsunami simulation by Model-A (teleseismic data) are considerably lower than the observed ones in the Sanriku coast. However, the simulated tsunami heights by Model-B (strong-motion data) correspond with the observed heights. On the other hand, the computed tsunami heights from both Model-A and Model-B are well consistent with the observed tsunami heights along the coast of the Sendai Plain.

We also present the tsunami inundation around the Soma Port by the tsunami simulation in the region E whose grid size is 15 m. Fig.10 shows the inundation area computed from Model-A and Model-B, comparing with one measured by Geospatial Information Authority of Japan (GSI) [17]. The computed inundation area by Model-A and Model-B correspond with the measured area.

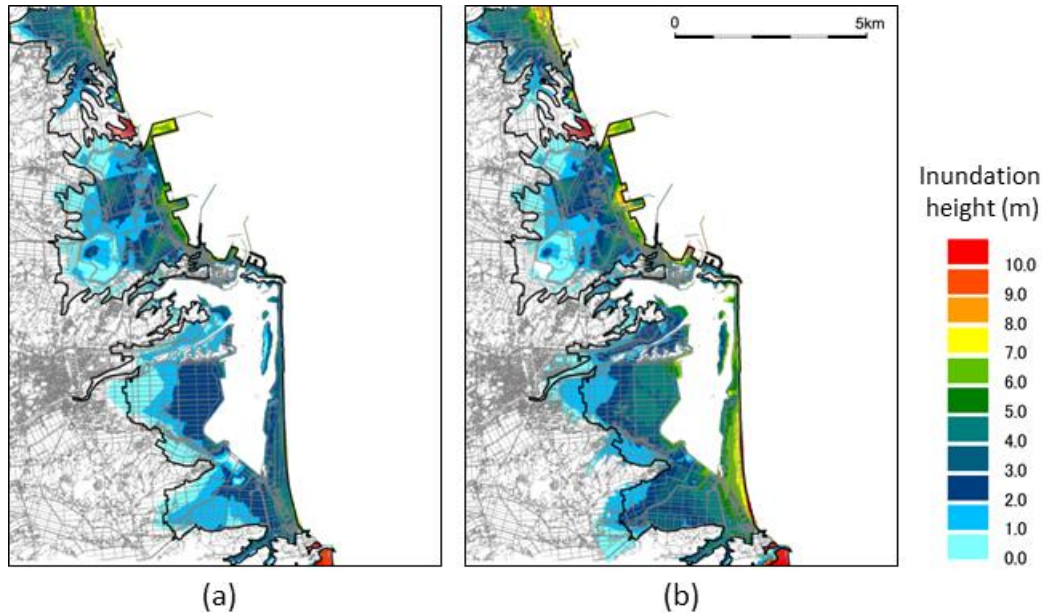


Fig.10 Distribution of inundation height by the tsunami simulation. (a) The inundation computed from Model-A (the teleseismic data). (b) The inundation computed from Model-B (the strong-motion data). Black line indicates the inundation area measured by GSI [17].

## 8. Discussion

Tsunami waveforms calculated by two types of the tsunami simulations are roughly similar to the GPS wave gauge data off the Pacific coast of Tohoku. However, in the Sanriku coast, the tsunami heights computed from Model-A based on the teleseismic data are fairly lower than the observed tsunami heights, while the computed heights from Model-B based on the strong-motion data correspond partly with the observed ones. In addition, the tsunami heights computed from Model-B are lower than the observed heights in the northern Sanriku coast. On the other hand, the coastal tsunami heights from two types of the tsunami simulations are consistent with the observed heights in the coast of the Sendai Plain, and the computed inundations around the Soma Port by the two tsunami simulations are similar to the observed one.

Satake et al. (2013) [6] indicate that a wide tsunami inundation in the Sendai Plain is due to a large slip on deep part of the plate interface and that the large slip near the trench axis is responsible for the large coastal tsunami heights along the Sanriku coast. They also point out that the large slip near the trench axis delayed for 3 min affects the largest tsunami heights in the northern Sanriku coast. We review the results of our tsunami simulations, based on their indication.

The computed coastal tsunami heights in the Sendai Plain and the inundation around the Soma Port by Model-A and Model-B are well consistent with the observed tsunami heights, because a large slip is generated on the deep part of the fault plane in both source models. The tsunami heights in the Sanriku coast computed from Model-A are lower than the observed heights, because the slip near the trench axis in Model-A is not so large. On the other hand, the computed tsunami heights in the middle and southern Sanriku coast by Model-B correspond with the observed heights, because there is a huge slip near the trench axis in this model. However, the tsunami heights in the northern Sanriku coast computed by Model-B are smaller than the observed ones, because there is no large slip near the trench axis delayed for 3 min toward north in Model-B.



A large slip near the trench axis, which causes huge tsunami heights in the Sanriku coast, arises in “tsunami earthquake” like the 1896 Sanriku earthquake. The tsunami earthquake does not bring out very strong ground-shaking. Therefore, it is difficult for Model-A based on the teleseismic data to reproduce the large slip along the trench axis, because the teleseismic observation that is measured far from the hypocenter is hard to detect the weak ground-shaking due to the large slip. On the other hand, Model-B based on the strong ground-motion data is able to roughly reproduce a large slip near the trench axis, because the strong-motion observation that is carried out near from the hypocenter can partly catch the weak ground-shaking caused by the large slip. It is one of future tasks to detect the weak ground-shaking, which is caused from a large slip near the trench axis, using the teleseismic or strong-motion observation systems with higher accuracy.

## 9. Conclusion

We carried out the tsunami simulations using the seabed displacements which were calculated from the ground-motion simulations for the 2011 Tohoku Earthquake. First, the large-scale simulations of ground motion by the voxel type finite-element method were performed for the Eastern Japan. In these simulations, two types of seismic source models were used; one was Model-A based on the teleseismic data, the other was Model-B based on the strong-motion data. Next, the tsunami simulations were executed by the finite-difference method based on the shallow-water theory, to obtain tsunami waveforms, coastal tsunami heights and inundation. The initial water level of the tsunami was assumed to be equal to the vertical displacement of seabed due to the fault slip, which was obtained from the ground-motion simulation.

Simulated ground-motion waveforms from two types of the seismic source models are mainly consistent with the observed ones at K-NET and KiK-net stations. These results represent that two types of the ground-motion simulation are carried out appropriately. Although the vertical displacement distributions obtained from two types of the ground-motion simulations appear depending on the slip distributions of the source models, those are roughly consistent with the one by Ozawa et al. (2011) [7].

Tsunami waveforms from two types of the tsunami simulations roughly correspond with the observed ones for phase and arrival time, at the GPS wave gauge stations. There are two features to point out for the simulated tsunami waveforms. First, the tsunami waveform simulated from Model-A based on the teleseismic data is primarily made of the long period component, because it is affected more greatly by a large slip in the deep part of the fault plane. Second, the short period component is dominant in the tsunami waveform simulated from Model-B based on the strong-motion data, because it is affected more strongly by a large slip in the shallow part of the fault plane near the Japan Trench.

Computed coastal tsunami heights in the Sendai Plain and computed inundation around the Soma Port from Model-A and Model-B are well consistent with the observed heights and inundation, because large slips are generated suitably on the deep part of the fault plane in both models. The tsunami heights in the Sanriku coast computed from Model-A are fairly lower than the observed heights, because the slip near the Japan Trench is not so large. On the other hand, the computed tsunami heights in the middle and southern Sanriku coast from Model-B correspond with the observed ones, because there is a huge slip near the trench axis in this model. However, the tsunami heights in the northern Sanriku coast computed by Model-B are smaller than the observed ones, because there is no large slip near the trench axis in Model-B, which is delayed for 3 min and propagates toward north. A large slip on the shallow part of the fault plane near the Japan Trench, which affects large tsunami heights in the Sanriku coast, is hard to be detected by the seismic observation because of lack of strong ground-shaking. It is desirable to reproduce the large slip near the trench axis by detecting the weak ground-shaking in the teleseismic or the strong-motion observation with higher accuracy.

In addition, it would be meaningful to compare the computed tsunami waveforms to the observed ones at the wave and tide gauges along the Pacific coast of Tohoku for advancing our approach in more detail. It is an issue that is left in the future.

## Acknowledgements

We thank Yasuhiro Yoshida and his co-workers for providing their source model derived from the inversion analysis of the strong motion records for the 2011 Tohoku Earthquake. The observed seismic waveforms used in this study are recorded at K-NET and KiK-net stations deployed by the National Research Institute for Earth



Science and Disaster Prevention (NIED). The observed tsunami waveforms used in this study are recorded at GPS wave gauges deployed in the Pacific Ocean by Nationwide Ocean Wave information network for Ports and HarbourS (NOWPHAS). We also use the coastal tsunami heights put in Japan Tsunami Trace Database by Tohoku University and the inundation heights measured by Geospatial Information Authority of Japan (GSI).

## References

- [1] Kinoshita S. (1998): Kyoshin net (K-NET), *Seismol. Res. Lett.*, 69, 209–332.
- [2] Aoi S., K. Obara, S. Hori, K. Kasahara and Y. Okada (2000): New strong-motion observation network: KiK-net, *Eos Trans. AGU*, 329.
- [3] Simons, M., S. E. Minson, A. Sladen, F. Ortega, J. L. Jiang, S. E. Owen, L. S. Meng, J. P. Ampuero, S. J. Wei, R. S. Chu, D. V. Helmberger, H. Kanamori, E. Hetland, A. W. Moore, and F. H. Webb (2011): The 2011 magnitude 9.0 Tohoku-Oki earthquake: Mosaicking the megathrust from seconds to centuries, *Science*, 332, no. 6036, 1421–1425.
- [4] Ide, S., A. Baltay, and G. C. Beroza (2011): Shallow dynamic overshoot and energetic deep rupture in the 2011 Mw 9.0 Tohoku-Oki earthquake, *Science*, 332, no. 6036, 1426–1429.
- [5] Yoshida Y., H. Ueno, D. Muto and S. Aoki (2011): Source process of the 2011 off the Pacific coast of Tohoku Earthquake with the combination of teleseismic and strong motion data, *Earth Planets Space*, 63, 565–569.
- [6] Satake K., Y. Fujii, T. Harada and Y. Namegaya (2013): Time and space distribution of coseismic slip of the 2011 Tohoku Earthquake as inferred from tsunami waveform data”, *Bull. Seism. Soc. Am.*, Vol.103, 1473-1492.
- [7] Ozawa S., T. Nishimura, H. Suito, T. Kobayashi, M. Tobita and T. Imakiire (2011): Coseismic and postseismic slip of the 2011 magnitude-9 Tohoku-Oki earthquake”, *Nature*, 475, 373-376, doi: 10.1038/nature10227.
- [8] Okada Y. (1985): Surface deformation due to shear and tensile faults in a half-space, *Bull. Seism. Soc. Am.*, 75, 1135-1154.
- [9] Ohmachi T., H. Tsukiyama and H. Matsumoto (2001): Simulation of tsunami induced by dynamic displacement of seabed due to seismic faulting, *Bull. Seism. Soc. Am.*, 91, 9, 1898-1909.
- [10] Furumura T. and T. Saito (2009): Integrated ground motion and tsunami simulation for the 1944 Tonankai earthquake using high-performance supercomputers, *Journal of Disaster Research*, Vol.4, No.2, 118-126.
- [11] Akiyama S., K. Kawaji, M. Korenaga, S. Fujihara and T. Tamiya (2012): Tsunami simulation using vertical displacement calculated from simulation of ground motion due to seismic source model, *Journal of Japan Association for Earthquake Engineering*, Vol. 12, No. 4, Special Issue : The 2011 Great East Japan Earthquake (1), p.4\_308-4\_318 (in Japanese with English abstract).
- [12] Akiyama S. and K. Kawaji (2014): Simulation of Tsunami due to Seabed Displacement Obtained by Computed Seismic Ground Motion, *Second European Conference on Earthquake Engineering and Seismology*, Istanbul, Aug. 25-29, No.444.
- [13] Koketsu K., H. Fujiwara and Y. Ikegami (2004): Finite-element simulation of seismic ground motion with a voxel mesh”, *Pure Appl. Geophys.*, 161, 2463-2478.
- [14] Koketsu K., H. Miyake, H. Fujiwara and T. Hashimoto (2008): Progress towards a Japan integrated velocity structure model and long-period ground motion hazard map, *The 14th World Conference on Earthquake Engineering*, Beijing, China.
- [15] Imamura F., A. C. Yalciner and G. Ozyurt (2006): Tsunami Modelling Manual, International Research Institute of Disaster Science, Tokoku University (<http://www.tsunami.civil.tohoku.ac.jp/hokusai3/J/projects/manual-ver-3.1.pdf>, referred to on April 15, 2016).
- [16] Iwabuchi Y., H. Sugino, F. Imamura, Y. Tsuji, Y. Matsuoka, K. Imai and N. Shuto (2012) : Development of Tsunami Trace Database with Reliability Evaluation on Japan Coasts, *Journal of Japan Society of Civil Engineers*, Ser. B2 (Coastal Engineering), Vol. 68, No. 2 p. I\_1326-I\_1330 (in Japanese with English abstract).
- [17] Nakajima, H. and M. Koarai (2011): Assessment of tsunami flood situation from the Great East Japan earthquake, *Bull. Geosp. Inf. Auth. Jpn.* 59, 55–66.